Laboratory Tests of Rolling Resistance of Different Tread Profiles for the Wheel of Martian Rover

Michał Gorzym[1*], Damian Markuszewski[1]

[1] Department of Fundamentals of Machine Design and Operation, Warsaw University of Technology, Faculty of Automotive and Construction Machinery Engineering, Ludwika Narbutta 84, 02–524 Warsaw, Poland

* Corresponding author's e-mail: michal.gorzym@pw.edu.pl

ABSTRACT

The aim of the research was to design and build a research stand that can be used to compare different types of tire tread profiles of the Mars rover (made using 3D printing) and to select the one that meets the criterion of the lowest power consumption of the drive motor, which corresponds to the minimum rolling resistance in paved area. As part of the task, a research stand was designed and built, consisting of two drive units of the tested drive system: one as a driving unit, the other as a driven unit, generating resistance when rolling one tire after another. During the tests, the following parameters were measured: the amplitude of the supply current, the rotational speed, information about which was obtained from the motor controller and the encoder located in the BLDC (brushless direct-current) motor, and their variability over time. Additionally, the amplitude of the force pressing the wheel against the supporting surface, which generated tire deflection, was also measured. A relationship was demonstrated between the type of tire tread used, the force pressing the tires against the supporting surface and the rolling resistance forces of the Mars rover tires. The tire with the lowest rolling resistance under given operating conditions was selected.

Keywords: martian rover, rolling resistance, tire tread pattern, signal analysis, BLDC motor diagnostics.

INTRODUCTION

A moving vehicle is affected by forces counteracting movement. These include, primarily: aerodynamic resistance force, elevation resistance force, rolling resistance force, inertia force and internal resistance force. The Mars rover is a special vehicle, it moves at a low speed of up to 1 m/s, exploring the surroundings and accompanying the astronaut. In further analysis, air resistance can be omitted. The weight of the vehicle is precisely determined by the rules of the competition, so the force of inertia will be approximately constant. A small number of elements in the drive system generate negligible internal resistance. Grade resistance mainly depends on the slope angle, and in the case of obstacles on the competition track it is horizontal. One

of the most important factors affecting vehicle movement is rolling resistance. The Mars rover must have an energy monitoring system during the ERC competition [1].

The tyres used in automobiles, an example of which is shown in Figure 1 are built using parts with different properties. Some elements of the tyre (tread, arm, side) are used to provide flexibility and assumed damping, and the other ones (steel belt/belts, cords) are used to assure directional stiffness and form when under specific loads. A wide range of materials are used to manufacture the tyre and its components. One of distinguished element is the so-called steel belt. It consists of steel elements, which resemble sections of simple wire, but they are often made by twisting two or even more wires to add rigidity. The name "steel belt" is confusing because it is not a belt in the common sense but rather

Figure 1. A special off-road vehicle - the MB-191 Mars rover [1]

a number of layers of steel wire with diameter varying from 0.1 mm up to 0.5 mm. In every layer the single wires or twisted wires are arranged parallel and embedded in rubber. There are at least two sheets lying one on top of the other. The wires in one sheet are aligned at a specific angle to the wires in the other sheet. When viewed from above, it looks like a mesh, which buckles the tyre [2].

Depending on the shape of the surface, many tyre tread variants can be used for this type of vehicle. The division of tyres depending on the design of the tread pattern, as well as the method of marking this pattern, is presented in Table 1:

For the purposes of the measurements carried out as part of this article, the following formulas were selected: off-road (modified into a V-shaped profile) and driving. Additionally, a directional tyre with an oblique rib arrangement and a block tread pattern tyre with block-shaped studs.

Thermoplastic polyurethanes (TPU) are linear segmented block polymers which are prone to microphase separation due to the thermodynamic incompatibility between hard polar

Table 1. Example of the division of tyres depending on the design of the tread pattern [3]

Tread pattern	Pattern symbol	Example of tread pattern shape
Road	D	
Off-road	T	
Universal	U	
Driving	AN	
Leading	ANP	
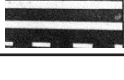
segments and relatively soft nonpolar segments. Compared with traditional processes, 3D printing technology can directly fabricate products with complex structures without application of moulds, which are difficult to obtain using traditional processes. The application of 3D printing technology to the manufacture of non-pneumatic tyres may not only greatly increase the freedom of non-pneumatic tyre structure design, but also quickly verify the feasibility of tyre structure design [4]. The subject of the analysis is the tyre of the drive unit of the MB-191 vehicle, whose task is to drive in specially prepared terrain, the geological and terrain conditions of which correspond to the planet Mars (except for temperature and gravity). The authors of the study undertook an attempt to build a test stand for investigating the rolling resistance of the wheel of a Martian rover competing in the international European Rover Challenge (ERC).

MATERIALS AND METHODS

The dominant surface type is sand: loose or marshy, as well as damp areas. Due to the low speed, it was decided to replace conventional inflated tyres with a solid tyre printed from TPU elastomer with mechanical properties similar to rubber, the internal structure of which is a cubic mesh with 30% filling. This ensures the flexibility of this tyre and cushioning as in a conventional inflated rubber tyre, while at the same time ensuring much lower weight. The most common tread shapes for off-road tyres were tested at a laboratory test stand. A measure based on the analysis of the drive motor supply current was developed, reflecting the level of rolling resistance. An experiment was conducted to verify the obtained results, determine the static and dynamic coefficient of friction of the tested polymer tyres. Research carried out the measurement of as many operating parameters of the off-road special vehicle drive system as possible, and then to verify the results obtained by means of a separate experiment. To carry out tests on tyres printed from TPU filament, it was not possible to directly transpose conventional methods of testing vehicle tyres. TPU filament is characterized by rubber-like properties, but it is a much stiffer and deformable structure in a different way than the case with typical rubber compound tyres. The decision to change the tyre from

inflated to solid was made after considering the following criteria [1]:
- low vehicle speed – maximum speed of 1 m/s;
- damping: due to the low weight of the vehicle (50 kg) and low driving speeds, it is not necessary to obtain such a high value of tyre damping as in the case of a conventional one;
- temperature: minimal heating during a drive on a paved surface;
- dimensional limitations: the printing area of the Ender V2 printer (210×210 mm) is the external limitation, and the engine body with gearbox in the drive wheel is the internal limitation;
- there is no risk of puncturing the tyre as a result of driving over a sharp-ended surface element (flexibility of the TPU material).

The tests stand measurements were divided into two main stages – preliminary tests, which allowed for detecting and eliminating the symptoms of damage to the BLDC motor winding (which caused errors and discrepancies in parameter readings) and additionally constituted a reference point regarding the order of magnitude of the measured parameters which the authors of the experiment are dealing with, which permitted appropriate matching of the graphs and spectra data with each other for comparative purposes and the final general tests. The basic tests included a full spectral analysis of the measured values on all available measurement channels: BLDC motor supply current, rotational speed from the encoder, pressure-generating force, which caused deflection of the tyre during movement, vibrations at the workstation, and changes in the sound pressure level during operation of the bench. In the course of test stand research, the following measurements were carried out:
- amplitude of the current feeding the BLDC motor controller;
- amplitude of the voltage signal corresponding to the rotational speed from the motor encoder;
- force pushing the drive unit against the resisting surface, generating resistance during operation;
- vibration amplitudes of the drive unit;
- variations in sound pressure levels at the test stand during operation.

The tests were carried out for a constant tyre deflection value. By assumption, they were comparative, and their purposes included:

- an attempt to estimate rolling resistance based on the current signal for each tread profile,
- an attempt to demonstrate the impact of changing the type of tread on the wheel-to-wheel interaction and on the speed and current characteristics of the BLDC motor, diagnosis of possible failures of the measuring system and assessment of the stiffness of the measurement test stand.

The next step was to calculate the actual rotational speed of the engine based on the encoder signal for all tyres and deflections for high and low rotational speeds (characteristic parameters).

Analysing the spectra and find the frequencies characterising the operation of the test stand, such as harmonics (rotational speed, supply current, gear mesh frequency) at the first and second stage, it was necessary to find the exact value of the rotational speed in the particular case under analysis. During the experiment, the speed settings on the controller were the same both for low and for high rotational speeds. However, since the setting was manual up to the marked indicator and the tyre profiles differed (resulting in differences in rolling resistance) depending on the tyre deflection, the wheel speeds differed slightly from each other in subsequent cases.

In connection with the above fact, a decision was made by the authors of this article to obtain accurate information about the current rotational speed of the wheel at the time of a specific measurement based on the reading of information from the encoder signal of this engine. Due to the large number of measurement points (sampling frequency f_p = 25 kHz), an algorithm prepared in the MATLAB program was developed. With its help, the number of spots where the signal passes through 0 was determined using the built-in procedure of the dsp. Zero Crossing Detector program from the DSP System Toolbox library. This number – characteristic for each measurement – was then used in the calculation of the rotational speed of this engine.

Initially, the number of passes through 0 was determined on the basis of counting the spots of changing the signal sign (in the theoretical case of the signal, this would be possible because it would be in the form of a perfectly rectangular signal). However, because the measured and analysed signals are real – the waveform of the signal does not correspond perfectly to the theoretical one, and there are intermediate bends on

the rising and falling slopes and signal extremes, which, counted by the original version of the program, resulted in an incorrect reading of the later calculated rotational speed. For the purposes of further analysis, the following calculation formula for engine speed was developed:

$$n_{obr} = \frac{x \cdot u}{3 \cdot p} \qquad (1)$$

where: x – the number of transitions of the encoder signal through the axis of abscissas for a 10-second measurement;
$u = 6$ – the number of windings (magnets) of the BLDC motor;
$p = 4$ – the number of pairs of poles of the BLDC motor;
3 – the number of phases of the electric motor.

Verification of the speed calculation method using the above method was carried out using the empirical method – using a tachograph gauge, applied directly to the rotating shaft of the drive motor. Based on the tachometer readings for low and high-speed settings (the same as for stationary measurements), it was concluded that the actual readings correspond to the values calculated. Hence, the developed method of converting the number of encoder signal bands to [rpm] may be considered correct.

In order to be able to compare the results of parameter measurements for drive systems with different tyres in a universal way, a comparative measure – the change in the width of a single PWM signal band (which, with respect to the motor's constant speed and signal period, induces a measure in the form of a change in the fill level of the PWM signal as this measure) and the load on this motor (electricity consumption) – was noticed and determined.

To obtain information about the type of gearbox used inside the electric motor, it was disassembled. The planetary reduction gear with a gear ratio of 1:30 is made using Bakelite teeth, mounted on a metal wheel, transmitting torque from one gear stage to the other. The planetary gear housing (in this case the motor housing – the black element on the right side of the Figure 2) is stationary.

In order to analyse the results and spectra from the measurement channels recorded, acquiring a basic knowledge of the values characterising the operation of single- and two-stage gearboxes was required. The tested vehicle wheel drive

Figure 2. Two stages of the planetary gear of Diam57 NEMA23 motor

system is equipped with a 4-pole, 3-phase 60W BLDC motor of the Diam57 type at 24V (OE: PB60630391) with permanent magnets and a two-stage planetary gearbox with a total ratio of 1:30 (1:10 at stage I and 1:3 at stage II). The number of teeth of the first-stage gears is respectively: z1 = 8, z3 = 72, while at the second-stage gears: z1 = 35, z3 = 72.

The formulas used to calculate the frequencies characterizing the planetary gearbox (Fig. 2) [5]:

$$f_{meshing \ I-stage \ planetary \ gearbox} = \frac{n_1 \cdot z_1 \cdot z_3}{60(z_1 + z_3)} \quad (2)$$

where: $z_1 = 8$ and $z_3 = 72$.

$$f_{meshing \ II-stage \ planetary \ gearbox} = \frac{n_1 \cdot z_1}{60(z_1 + z_3)} \quad (3)$$

The final step is the spectral analysis of measurements: current, rotational speed, vibration signals, and changes in the sound pressure level at the test stand. This is followed by the calculation of the contact area and tyre footprint for the deflections defined in the measurement plan: 0.5 mm, 1 mm, and 1.5 mm. For confidence and self-verification of the measurements made, a verification experiment was performed, which confirmed the results collected with the analytical method. The conclusions of the experiment include both observations and recommendations from the preliminary research and allow two specific types of TPU tyre shape to emerge, one optimal for driving at low speed and the other one at higher speeds.

LABORATORY STAND DESIGN

A decision was made to draw a preliminary test stand design in the SOLIDWORKS programme, using two drive units for the rover tested, in which the first wheel was driven in a stationary system and the other resisting wheel was mounted in a moving frame and pressed as a resisting surface by a screw (Fig. 3). Due to the construction of the vehicle under the requirements of the ERC Student 2022 competition, 80% of the rover competition arena (referred to as the "Mars yard") is hardstanding. For this reason, in the first stage of the research, the test stand was launched in laboratory conditions. Due to the initial assumption of completing the entire project on a possibly minimal budget, which could be covered by the scientific club's funds, all tasks were performed by the authors of the experiment themselves. Technical documentation with cost estimates was prepared for the structural and essential elements. Thanks to the implementation of the experiment in the Vibroacoustics Laboratory of the Faculty of Automotive and Construction Machinery, the costs related to the rental of signal analysis equipment manufactured by National Instruments and Brüel & Kjær were reduced to a minimum.

Additionally, authors recorded more potentially useful signals to analyse them in the future during more complex experiment. This signals are: bench vibrations – recorded by the Brüel & Kjær type 4514 accelerometer and changes in the sound pressure level during the operation of the test stand – recorded through a Brüel & Kjær type 4958 microphone. The laboratory test stand
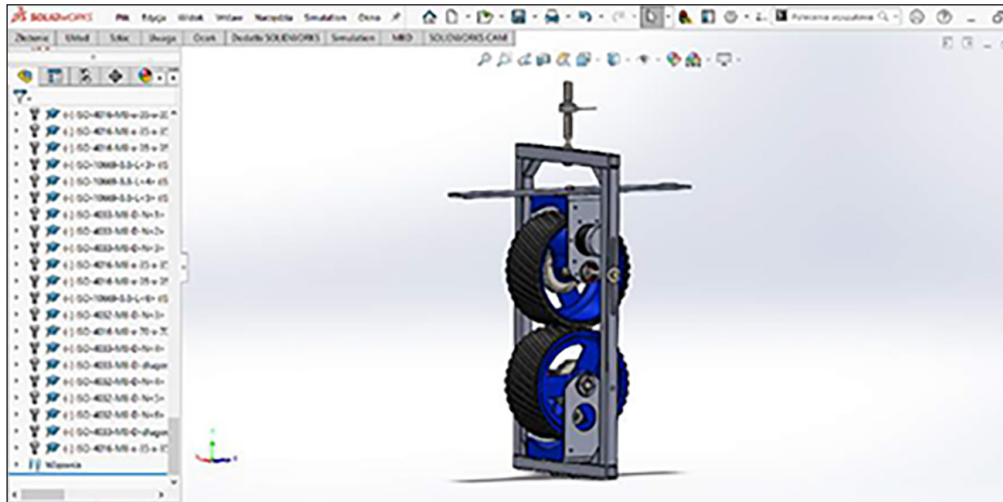
Figure 3. Design of the test stand developed in SOLIDWORKS – isometric view

(Fig. 4 and Fig. 5) in the version for preliminary tests was powered by a DC 24V lithium-ion battery (simulating real operating conditions during a drive over the ground). The use of direct current to power the components not only allowed for recreating the actual operating conditions of the drive systems as envisioned in the competition, but also made it possible to eliminate the impact of AC power disturbances from the building's grid, which is particularly important for preliminary research. In the next version of the tests at the test stand (the second part of the experiment),

the motor and measuring instruments were powered using a standard power supply grid.

RESULTS

By analysing the nature of the current waveform and the noticeable local extreme values at the points of disturbance of the rotational speed waveform, a theory emerged that there is an electrical breakdown at some point of the stator winding (Fig. 6 and 7). This was confirmed by reading

Figure 4. Test stand in laboratory conditions: 1 – KMM20 strain gauge load cell, 2 – rolling resistance test bench (Fig. 5), 3 – BLD-300B motor controller, 4 – 24V lithium-ion battery, 5 – NI eDAQ-9178 chassis for measurement systems with a multi-channel module equipped with NI 9234 and NI 9237 analogue-to-digital converters, 6 – PC with LabView Signal Express software

Figure 5. Measuring track in the laboratory

the "inf" voltage value on the NI measuring card supporting the +/- 5V range, while the motor supply voltage was 24V. The problem was eliminated by using plastic inserts between the winding elements, which prevented them from coming into contact again and generating an electrical breakdown. After eliminating potential sources of measurement interference (Fig. 6), the authors proceeded to the attempt at developing a calculation formula for two characteristic (from the point of setting the motor controller) rotational speeds, based on the PWM time signal depending on the mechanical parameters of this motor (number of windings, pairs of poles and phases of the electric motor) [6, 7].

The numbers of crossing points of the rotational speed signal with the value "0" and the rotational speeds of the electric motor determined on this basis are included in Table 2: n this experiment, in which a motor controlled by the level of filling the voltage signal is used, the increase in the load for the motor is directly proportional to the change in the width of the signal bands [6] from the encoder (Fig. 8). Based on the course of the engine speed and the number of 10 bands of this signal, the period of this signal was calculated. Subsequently, after dividing the period by the number of these bands, the width of a single signal band was determined, which is an indicator enabling a comparison of the current consumption (load) [7, 8] by the motor as the determinant of the tyre with the highest rolling resistance. Table 3 shows the results of the analysis of the rotational speed signal, and in the figure below the conventional reference of the width of a single band to the period of 10 signal bands. Figure 9 shows an example of the spectrum, which takes into account the mechanical parameters [9] calculated above,
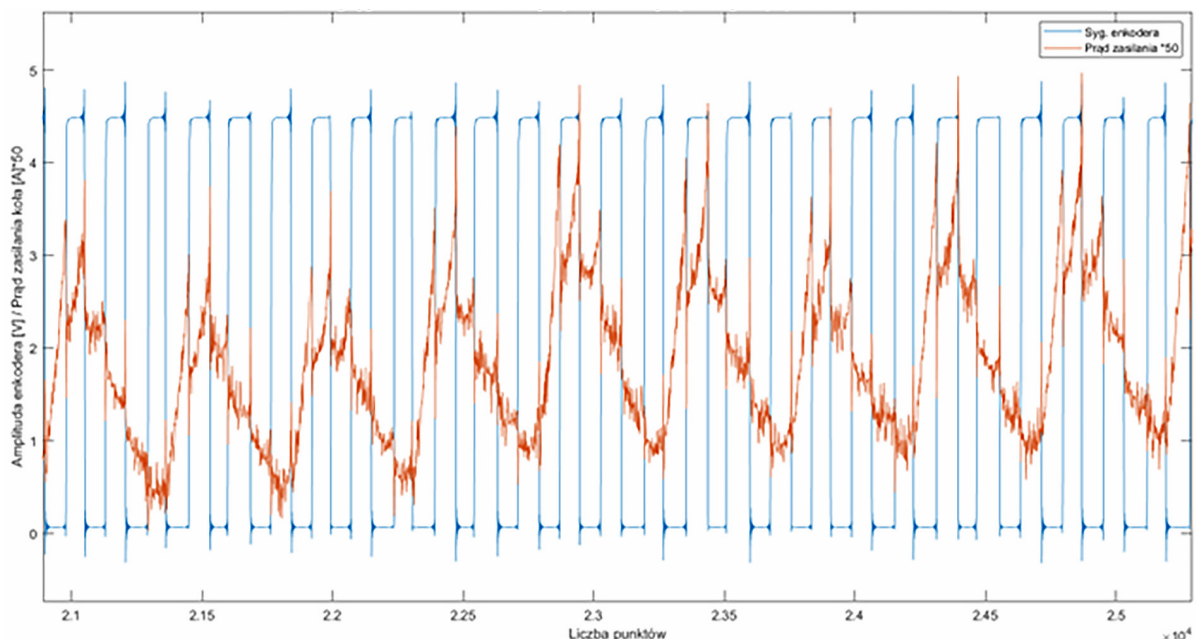

Figure 6. Waveform of the motor speed signal from the encoder with a scaled supply current waveform superimposed on it

Figure 7. NEMA 23 BLDC motor after dismantling the housing and exposing the windings. Visible residual insulation level of the windings (on the right)

Table 2. The results of calculations of the BLDC motor speed values based on information from the time course

Measurement file name	Number of zero spots of time signal	Engine shaft speed [rpm]	Engine shaft rotation frequency [Hz]
Kug1vM	3399	1944	32,4
Kug1vD	7169	3756	62,6
Kug2vM	3510	1755	29,25
Kug2vD	6819	3409.5	56.80
Kug3vM	2837	1418.5	23.64
Kug3vD	6147	3073.5	51.22
Nug1vM	3306	1653	27.55
Nug1vD	6949	3474.5	57.90
Nug2vM	3119	1559.5	25.99
Nug2vD	6717	3358.5	55.98
Nug3vM	2697	1348.5	22.47
Nug3vD	6359	3179.5	52.99
Sug1vM	2749	1374.5	22.90
Sug1vD	5206	2603	43.38
Sug2vM	2503	1251.5	20.86
Sug2vD	5558	2779	46.31
Sug3vM	1529	764.5	12.74
Sug3vD	5532	2766	46.10
Vug1vM	3390	1695	28.25
Vug1vD	7097	3548.5	59.14
Vug2vM	2893	1446.5	24.11
Vug2vD	6638	3319	55.32
Vug3vM	3096	1548	25.80
Vug3vD	6397	3198.5	53.31

Note: K – a tyre with a block tread profile; N – a tyre with a driving tread profile; S – a tyre with oblique tread ribs, V – a tyre with a V-shaped tread profile, ug1 – tyre deflection generated by 1 turn of the M8x1 nut (0.5 mm for two tyres), ug2 – tyre deflection generated by 2 turns of the M8x1 nut (1 mm for two tyres), ug3 – tyre deflection generated by 3 turns of the M8x1 nut (1.5 mm for two tyres), vM – low rotational speed, vD – high rotational speed.

characterizing the operation of the BLDC motor with the gearbox [10, 11]. The authors assumed that since the deflection increases, the contact area of a given tyre with the resisting surface will increase. An attempt to assess the area of this surface is the projection of the surface resulting from the intersection of the tyre [13] (with 4 designed tread variants) with a parallel plane (Fig. 10, Fig. 11), spaced from the ground for subsequent assumed deflections of 0.5, 1 and 1.5 mm. Below are examples of visualizations of adjacent surface calculations for 3 deflections.
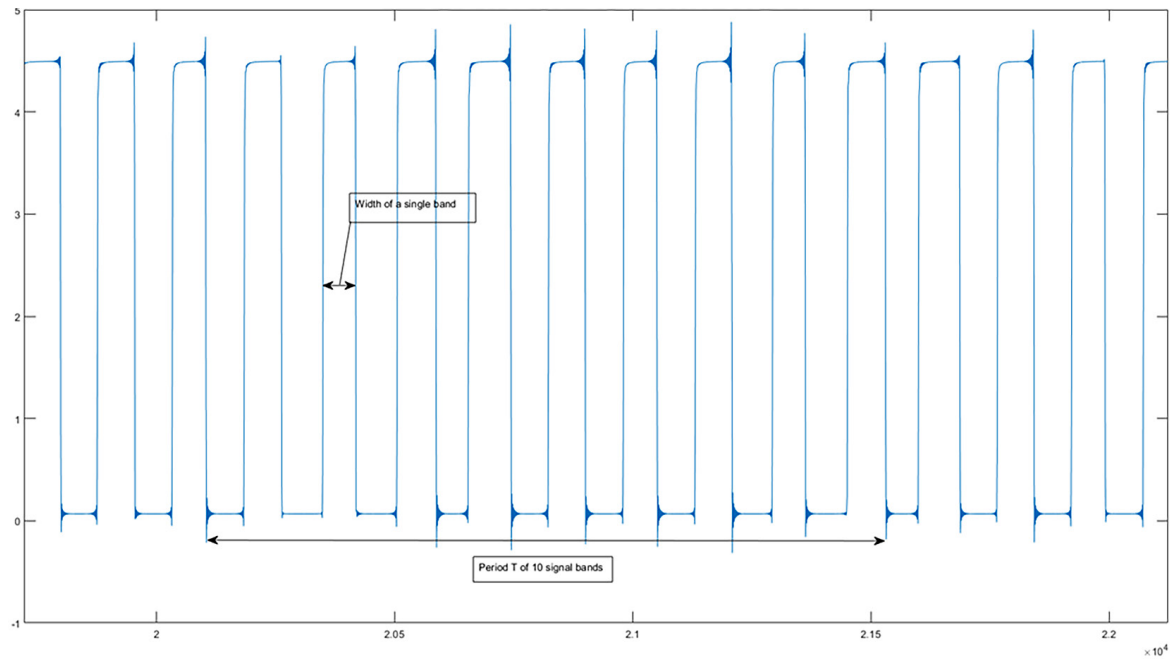
Figure 8. Encoder signal waveform – explanation of period T and the width of single band

Table 3. Results of the analysis of the width and period of the wheel speed signal bands

| Measurement file name	Width of 1 signal band [l. pkt.]	T signal period [l. pkt.]
Kug1vM	79	133
Kug1vD	34	61.7
Kug2vM	61	126
Kug2vD	37	68.8
Kug3vM	72	146
Kug3vD	39	69.1
Nug1vM	75	132.3
Nug1vD	37	65.7
Nug2vM	80	138.2
Nug2vD	39	69.7
Nug3vM	91	161.7
Nug3vD	40	71.9
Sug1vM	80	149.7
Sug1vD	48	82.6
Sug2vM	114	188.8
Sug2vD	42	80.1
Sug3vM	45	83.7
Sug3vD	50	85.3
Vug1vM	71	130.7
Vug1vD	34	62
Vug2vM	79	149.5
Vug2vD	35	63.9
Vug3vM	74	139.8
Vug3vD	37	69.4
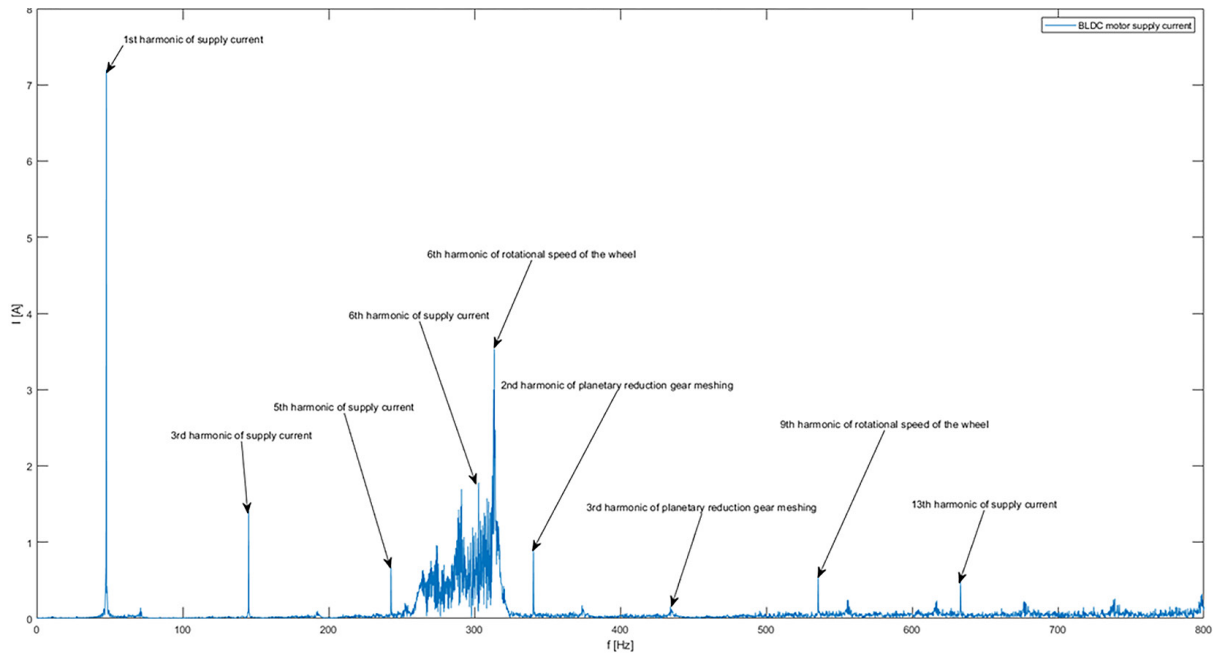
Figure 9. The spectrum of the BLDC motor power supply current with characteristic [12] electromechanical values (Table 4)

Table 4. Frequencies characteristic of individual tyre tread measurements, possible to make reference to on the spectra

Measurement name	Characteristic frequencies		
	$f_{\text{częst. prądu zas.}}$ (frequency of the supply current) = 48.8 Hz		
	First harmonic of the meshing frequency of the stage I of the planetary gearbox [Hz]	First harmonic of the meshing frequency of the stage II of the planetary gearbox [Hz]	Engine shaft rotation frequency [Hz]
Kug1vM	233.28	3.2	32.4
Kug1vD	450.72	6.26	62.6
Kug2vM	210.6	2.92	29.25
Kug2vD	409	5.68	56.80
Kug3vM	170.22	2.36	23.64
Kug3vD	368.82	5.12	51.22
Nug1vM	198.36	2.75	27.55
Nug1vD	416.94	5.8	57.90
Nug2vM	187.14	2.6	25.99
Nug2vD	403.02	5.6	55.98
Nug3vM	161.82	2.24	22.47
Nug3vD	381.54	5.3	52.99
Sug1vM	161.94	0.03	22.90
Sug1vD	312.36	4.33	43.38
Sug2vM	150.18	2.08	20.86
Sug2vD	333.48	4.63	46.31
Sug3vM	91.74	3.24	12.74
Sug3vD	331.92	4.63	46.10
Vug1vM	203.40	2.82	28.25
Vug1vD	425.82	5.91	59.14
Vug2vM	173.58	2.41	24.11
Vug2vD	398.28	5.53	55.32
Vug3vM	185.76	2.58	25.80
Vug3vD	383.82	5.33	53.31

Table 5 contains the values of the area of tyre contact with the ground in the form of calculating the projection area of the abscised fragment of a tyre onto the cutting plane [14]. Calculations in SOLIDWORKS were made for three considered tyre deflections: 0.5 mm, 1 mm and 1.5 mm.

In addition, calculations and graphs were prepared showing the dependence of the force generating tyre deflection on the size of this deflection and the rotational speed: low and high, as well as their average and maximum values, as shown in Tables 6–11.

Table 10 presents band width values and the spacing between the consecutive ten bands for both high and low rotational speeds.

The measure of the BLDC motor load during these measurements, (much like in motors controlled by the level of PWM signal filling), is the variation in the width of rotational speed signal band (Fig. 12) [11, 15]. This measure was referred to changes in the tyre deflection for a specific tread pattern in order to determine the relationship between the tyre tread pattern and the generated motor load. Based on the above mileage, it is evident that the lowest motor load is ensured by the V-shaped tread tyre. Then, the tyre with a block tread pattern exhibits comparable performance in the context of small deflections. The narrower the signal band width, the lower the signal duty cycle, thus
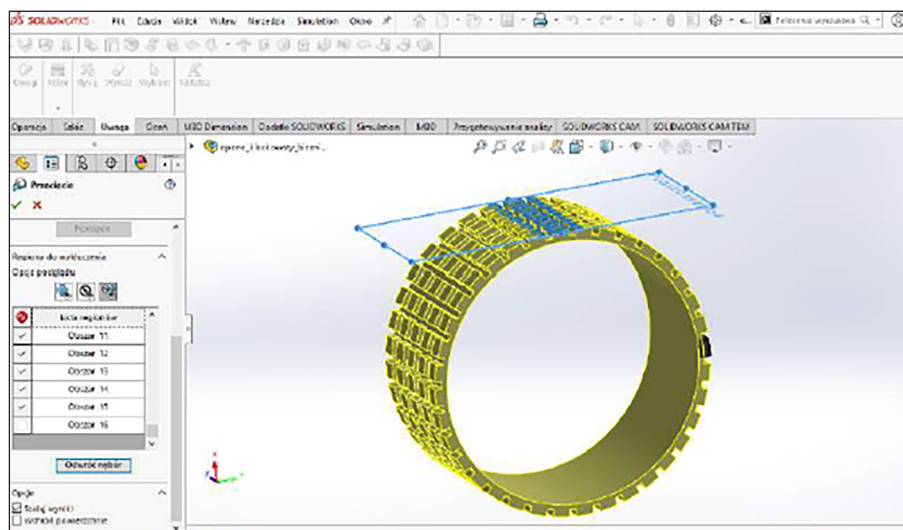

Figure 10. Calculation of the contact area for a tire with a block tread in SOLIDWORKS for given deflections of 0.5, 1 and 1.5 mm
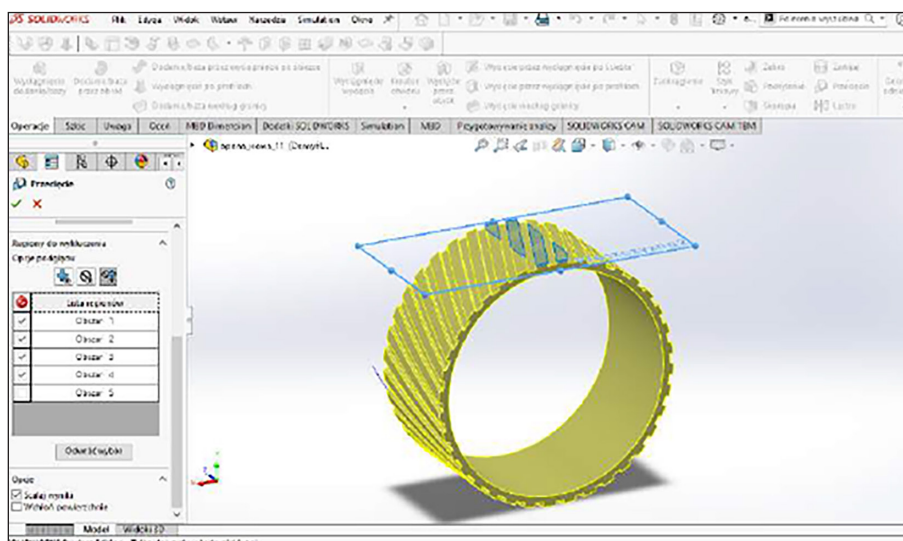

Figure 11. Calculation of the contact area for the tyre with an oblique tread profile for deflections of 0.5, 1 and 1.5 mm

Table 5. The values of the calculated areas of contact between the tyre and the ground for given tyre deflection values

Tyre type	Deflection 0.5 mm	Deflection 1 mm	Deflection 1.5 mm
	Contact area [mm²]		
Block tread	167.04	1141.35	1585.25
V-shaped tread	1494.38	2031.94	2443.96
Oblique pattern tread	1135.56	1612.99	1943.37
Drive tread	501.86	676.54	872.29

Table 6. Average tyre-ground contact force at low speed – 1944 rpm

Tyre type	Deflection 0.5 mm	Deflection 1 mm	Deflection 1.5 mm
	The value of contact force [N]		
Block tread	133.46	133.65	171.32
V-shaped tread	143.34	173.72	261.82
Oblique pattern tread	20.48	84.88	288.43
Drive tread	119.45	134.37	185.42

Table 7. Average tyre-ground contact force at high speed – 3319 rpm

Tyre type	Deflection 0.5 mm	Deflection 1 mm	Deflection 1.5 mm
	The value of contact force [N]		
Block tread	133.23	131.03	152.39
V-shaped tread	131.15	136.45	198.35
Oblique pattern tread	17.95	118.64	252.73
Drive tread	37.51	45.14	160.4

Table 8. Maximum tyre-ground contact force at low speed – 1944 rpm

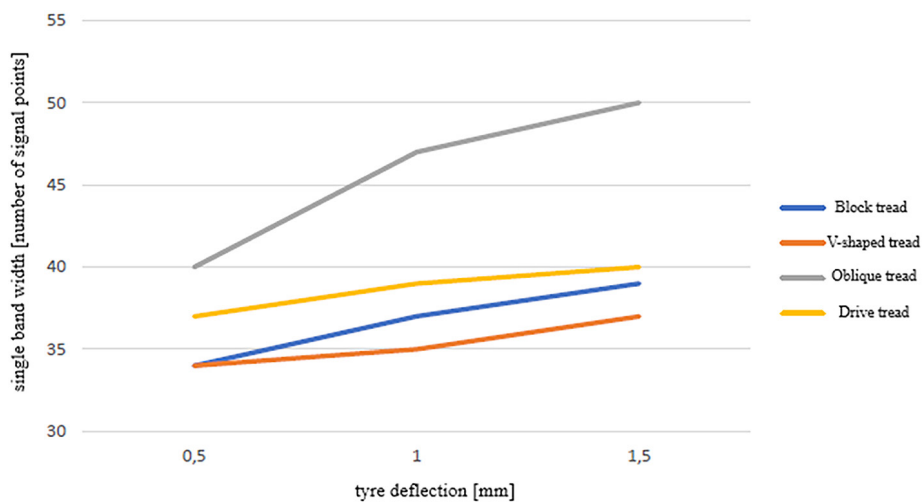| Tyre type	Deflection 0.5 mm	Deflection 1 mm	Deflection 1.5 mm
	The value of contact force [N]		
Block pattern tread	185.89	281.35	455.44
V-shaped tread	386.94	488.45	565.93
Oblique pattern tread	169.63	402.23	509.80
Drive tread	311.27	307.34	356.24

Figure 12. Correlation between electric energy consumption (determined by the width of a single pulse width modulation signal band) and tyre deflection

Table 9. Maximum tyre-ground contact force at high speed – 3319 rpm

Tyre type	Deflection 0.5 mm	Deflection 1 mm	Deflection 1.5 mm
	The value of contact force [N]		
Block pattern tread	176.2	274.08	427.26
V-shaped tread	238.98	414.63	462.66
Oblique pattern tread	248.95	486.38	602.45
Drive tread	161.77	311.92	384.12

Table 10. Signal band width based on deflection and tyre type at low speed – 1944 rpm

Tyre type	Deflection 0.5 mm	Deflection 1 mm	Deflection 1.5 mm
	Width of signal band [l. pkt.]		
Block pattern tread	66	70	72
V-shaped tread	74	77	79
Oblique pattern tread	80	104	188
Drive tread	75	80	91

Table 11. Width of signal band based on deflection and tyre type at high speed – 3319 rpm

Tyre type	Deflection 0.5 mm	Deflection 1 mm	Deflection 1.5 mm
	Width of signal band [l. pkt.]		
Block pattern tread	34	37	39
V-shaped tread	34	35	37
Oblique pattern tread	40	47	50
Drive tread	37	39	40

reducing the current consumption required to maintain the desired motor rotational speed [16].

VERIFICATION OF THE RESULTS

Additional experiments were conducted, assuming that it is possible to directly measure the rolling resistance force using a dynamometer through which the vehicle is pulled on a specific substrate. The same pattern applies when pulling tyres with various tread patterns on an undistorted substrate – in the case of this experiment, on linoleum, which exhibits similar characteristics to TPU filament, the material from which the tyres were made. Measurements were conducted for each of the described tread patterns. The total rolling resistance force of the vehicle F_T, is the sum of rolling resistances occurring on all car wheels:

$$F_T = F_{t1} + F_{t2} + F_{t3} + F_{t4} = \sum F_t \qquad (4)$$

where: $F_{t1...4}$ – are the rolling resistance forces of individual wheels of the vehicle, expressed in newtons.

The same force can be measured practically [3] by pulling or pushing the vehicle with the use of a dynamometer (Fig. 13). The ratio of the total force F_T to the total weight of the vehicle ($Q_{total} = m_{total} \cdot g$) is referred to as the rolling resistance coefficient, and is expressed by the formula:

$$f_t = \frac{F_T}{Q_c} = \frac{\sum F_T}{m_{całk} \cdot g} \qquad (5)$$

where: f_t – is the rolling resistance coefficient [-], m_{total} – is the total mass of the vehicle [kg].

In the area of the spring's contact surface, compression occurs sequentially (Fig. 10 and Fig. 11), while outside the ground contact area – decompression. After leaving the working area, dampers transform the energy into heat emission. The rolling resistance of the wheel is represented by the work L_w related to the distance travelled l_s by the wheel (Fig. 14).

$$F_T = \frac{L_w}{l_s} = z^2 \cdot (k \cdot \omega) \cdot \frac{\pi}{2} \cdot \frac{1}{l_s} \qquad (6)$$
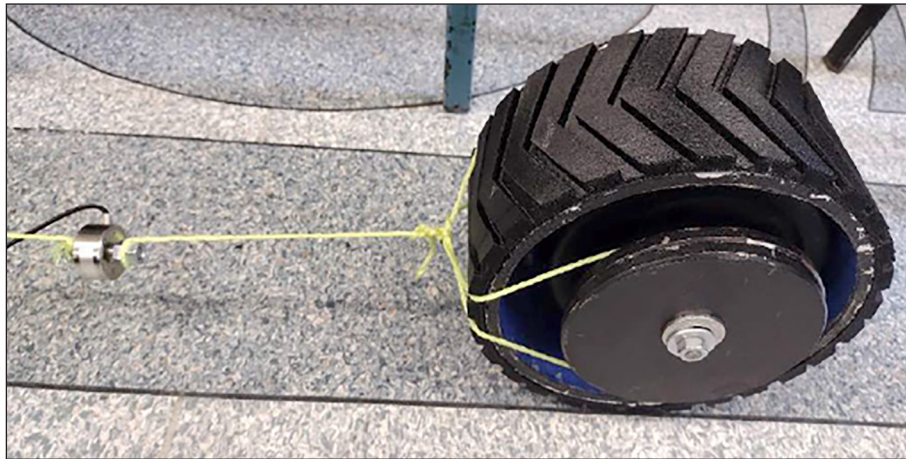
Figure 13. Verification: pulling the wheel using a dynamometer – V-shaped tread tyre

where: z – is the arrow of tyre deflection, k – is the tyre damping constant, and ω – is the angular velocity of the wheel [3].

Based on the above formula, it can be concluded that the resistance force is directly proportional to the square of the tyre deflection, which, in turn, depends on the tyre's construction (including the wheel, which is an integral part of it, as discussed in this article) The damping of the tyre and the entire wheel structure is closely dependent on the properties of the TPU elastomer and the flexibility of the 3D-printed wheel core, which, for enhanced durability, has been additionally coated with three layers of carbon fibre and Epidian 5 epoxy resin.

Through the introduction of the radial stiffness constant c, defined as the ratio of tyre load Q to its maximum tyre deflection z (c = Q/z) in the formulas (Fig. 14 and Fig. 15), the rolling resistance coefficient can be represented by the following Equation [1]:

$$f_t = \frac{\pi}{2} \cdot \frac{k \cdot \omega}{c} \cdot \frac{z}{l_s} \qquad (7)$$

Subsequently, comparative charts were created (Table 12), depicting the values of rolling resistance generated by each tyre. These are the values of the horizontal component of the total vehicle motion resistance, denoted by F_t. In contrast, the vertical component (F_z) depicted in Figure 14 is referred as the tyre contact or deflection-generating force and it was determined during measurements at the test stand.

The highest resistance is observed for the V-shaped tread tyre (Fig. 16), which results from
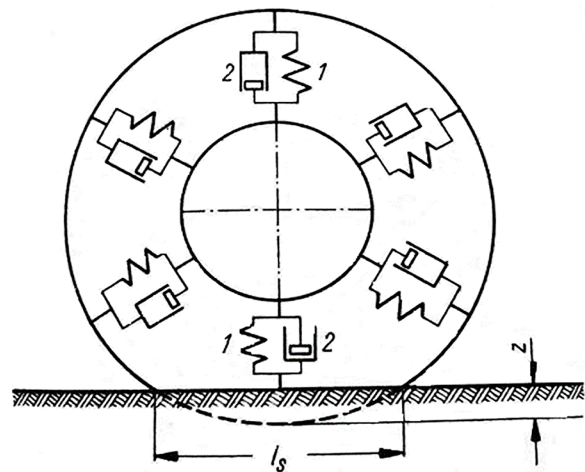

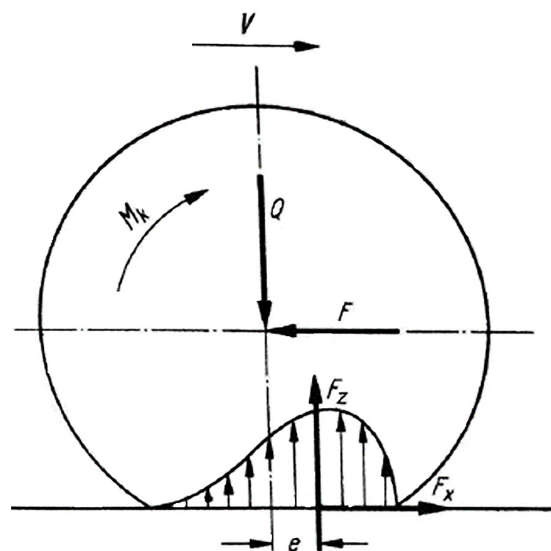**Figure 14.** A simplified tyre model that takes into account the parameters of elasticity and damping_V2

Figure 15. Longitudinal distribution of the normal reactions of the surface in the case of a rolling wheel loaded with torque [3]

293

Table 12. The values obtained for the experiment

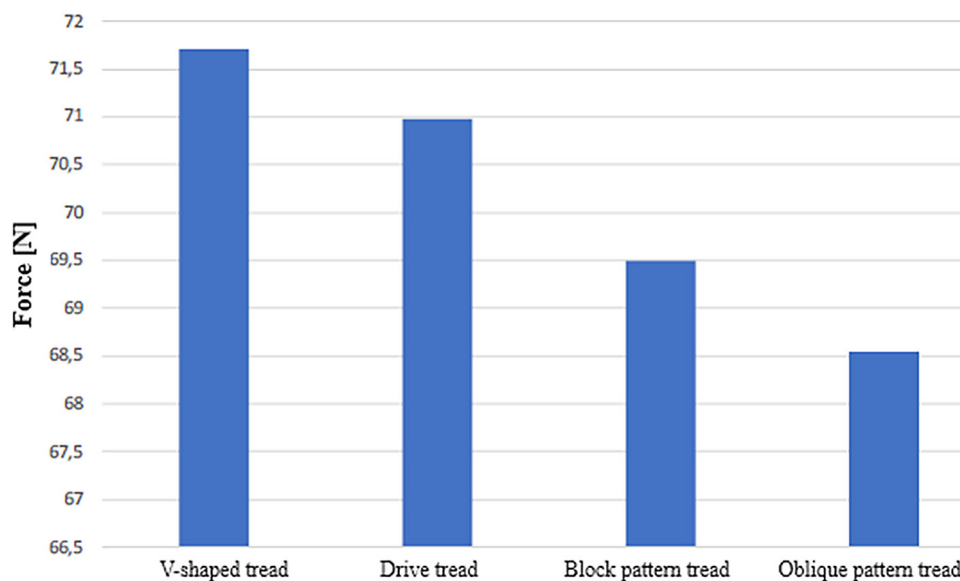| Tyre type	Maximum rolling resistance force [N]
Block pattern tread	69.49
V-shaped tread	71.71
Oblique pattern tread	68.54
Drive tread	70.98
Tyre type	Average rolling resistance force [N]
Block pattern tread	36.26
V-shaped tread	43.69
Oblique pattern tread	45.69
Drive tread	41.70

Figure 16. Chart showing the maximum tyre rolling resistance force based on the tyre type used

its larger contact area with the surface and the tread pattern. Unlike block or drive treads (which have larger spaces between tread elements), this pattern hinders the wheel's smooth movement on the surface due to the highest contribution of the rubber structure in the contact area.

CONCLUSIONS

The experiment revealed that the tyre with the lowest rolling resistance at a speed of 22 RPM (lower rotational speed) is the block tread tyre. In comparison, at a speed of 38 RPM (higher characteristic speed), the V-shaped tread tyre exhibits the lowest resistance. The results of comparative tests were confirmed by verification experiment, which consisted in pulling a loaded wheel on a non-deformable substrate, similar in properties to a driving wheel, from the test stand.

During the experiment, redundant signals were recorded such as acoustic signal from engine's planetary gearbox and vibrations signals. As a actual diagnostic symptom the rotational speed signal from BLDC motor was used. The width of the signal band, which can be related to the duty cycle factor is sensitive to changes in the load putted on the drive unit and in the case of this paper – rolling resistance. All of measurements were carried out for three constant deflection values, which means that the dynamic radius for each (non-pneumatic) tyres is constant as well. Changes inf the resultant vertical reaction force of the surface were observed. The measurements aimed to determine the optimal tread pattern for minimal rolling resistance, which subsequently contributes to minimal power consumption by the drive motor.

This aspect is continuously monitored during vehicle trials on the "Mars yard" test track during European Rover Challenge event.

REFERENCES

1. Podembski K. Suspension – internal materials of KN Bekker Team, Faculty of Automotive and Construction Machinery Engineering, Warsaw University of Technology. 2020; 3–8.

2. Brol S., Warczek J. Utilization of magnetic signature of automotive tire for exploitational wear assessment. Diagnostyka. 2022; 23(4), 1–3. https://doi.org/10.29354/diag/156255

3. Jaworski J. Tires for motor vehicles. Construction and operation. Wydawnictwo Komunikacji i Łączności. 1987; 47–49, 85–91. [In Polish].

4. Wang J., Yang B., Xiang L., Gao L., Lu Y., Wang R. Research of TPU materials for 3D printing aiming at non-pneumatic tires by FDM method. Polymers. 2020; 12(11), 1–19. https://doi.org/10.3390/polym12112492

5. Bartelmus W., Zimroz R. Planetary diagnostics method. Scientific Works of the Mining Institute of Wroclaw University of Science and Technology. 2017; 118 (33), 4–5. [In Polish].

6. Glinka T., Szymaniec S. Operation and diagnostics of electrical machines and transformers. Diagnostics of machines and devices – general comments. Napędy i Sterowanie. 2020; 22(5), 36–49. [In Polish].

7. Skóra M., Kowalski Cz. Analysis of vibrations in the drive with a PM BLDC motor caused by controller damage. Przegląd Elektrotechniczny. 2017; 93, 126–129. [In Polish]. https://doi.org/10.15199/48.2017.02.29

8. Definition of Brushless BLDC motor – principle of operation, application, advantages. Available at: https://www.ebmia.pl/wiedza/porady/automatyka-porady/silnik-bezszczotkowy-bldc-co-to-jest-jak-dziala-zastosowanie/ [Accessed: 16.12.2023]

9. Batko W., Dąbrowski Z. Modern methods of testing vibroacoustic processes (technical applications) part II, ITE – PIB 2006 [In Polish].

10. Ahnesjö H. Fault detection of planetary gearboxes in BLDC-motors using vibration and acoustic noise analysis. Uppsala Universitet, UPTEC E 20026 2020, 1–5, 7–9.

11. Lihong J., Junpeng S., Xigui W., Yongmei W., Baixue F. Vibroacoustic characteristics analysis of a planetary gear reducer considering the exterior housing structure. Mechanical Sciences. 2021; 12, 539–557.

12. Spectral analysis of random signals – definitions and applications. Available at: http://atol.am.gdynia.pl/tc/cps2007/analiza.html [Accessed 20.01.2024]

13. Konieczny Ł., Burdzik R., Warczek J., Wilk A. Proposal of using phase angle as a complement to vibration methods in the diagnosing of cars suspension systems. Przegląd Mechaniczny. 2016; 10, 37–41, https://doi.org/10.15199/148.2016.10.5

14. Andrzejewski R. Dynamics of the pneumatic road wheel. WNT Warszawa 2010, 36–37, 129–139. [In Polish].

15. Goyal D., Pabla B. The vibration monitoring methods and signal processing techniques for structural health monitoring: a review. Archives of Computational Methods in Engineering. 2016; 23, 585–594. https://doi.org/10.1007/s11831-015-9145-0

16. Miao Q., Zhou Q. Planetary gearbox vibration signal characteristics analysis and fault diagnosis. Shock and Vibration. 2015; 126489, 3–8. http://dx.doi.org/10.1155/2015/126489